https://doi.org/10.1016/j.apenergy.2016.06.064

Modeling of Direct Carbon Solid Oxide Fuel Cell for CO and Electricity Cogeneration

Haoran Xu[1], Bin Chen[1], Jiang Liu[2], Meng Ni[1,*]

[1] Building Energy Research Group, Department of Building and Real Estate
The Hong Kong Polytechnic University, Hung Hom, Kowloon, Hong Kong, China
[2] New Energy Research Institute, School of Environment and Energy, South China University of Technology, Guangzhou 510006, PR China

Abstract:

Direct Carbon Solid Oxide Fuel Cell (DC-SOFC) is a promising energy conversion device for power generation using solid carbon fuel. In this paper, a 2D model is developed for a tubular DC-SOFC for CO and electricity co-generation. Parametric simulations are conducted to understand the physical/chemical processes in the DC-SOFC. Good performance of DC-SOFC is observed even at a large distance between the carbon bed and the porous anode, indicating the feasibility of large-scale DC-SOFC applications. The DC-SOFC performance is found to decrease with decreasing temperature due to the decreased Boudouard reaction kinetics. It's also found that the molar fraction of CO at the anode can be well controlled by adjusting the operating conditions, enabling DC-SOFC for electricity and CO cogeneration. Another finding is that the current density in the DC-SOFC increases slightly along the cell length, which is different from the H_2-fueled SOFC. In addition, the anode-supported configuration is found to be beneficial in improving the electrical output of the DC-SOFC but is unfavorable for CO generation. A small D_{ce} and a high potential are recommended to improve CO generation from the DC-SOFC. The model can be used for design optimization of DC-SOFC at a system level.

Keywords: Solid oxide fuel cell (SOFC); Carbon; Cogeneration; Mathematical modeling;

* Corresponding author:
Email: bsmengni@polyu.edu.hk; Tel: 852-27664152; Fax: 852-27645131.

1. Introduction

1.1. Works done before

Carbon is the major component of fossil fuels. It can also be obtained from renewable biomass such as waste wood. The solid carbon fuel is commonly used for electricity generation in conventional thermal power plants which produce pollutants and hazardous gases such as CO_2, SO_x and NO_x [1]. In addition, the efficiency of power generation by thermal power plant is only about 40% due to the Carnot efficiency limit and the various losses involved in the thermodynamic cycle. Therefore, more efficient energy conversion and better emission control for energy conversion using carbon fuel are critical since carbon-based fuel will continue to be the major energy source in the coming decades.

Solid oxide fuel cell (SOFC) is an electrochemical device which can convert the chemical energy of a fuel into electrical energy at efficiency higher than that of a conventional thermal power plant. It is a whole solid-state device with an oxygen-ion-conducting electrolyte being sandwiched between two porous electrodes [2]. As the fuel and oxidant are separated by the dense electrolyte, emission control in SOFCs is relatively easy. As the operating temperature of SOFC is high (about 800^{o}C), electrochemical reactions are fast, enabling the use of low cost catalyst such as Ni. For comparison, low temperature fuel cells such as proton exchange membrane fuel cells (PEMFCs) usually need expensive noble-metal catalyst such as Pt. In addition, SOFCs are fuel flexible and can use not only H_2, but also various hydrocarbon fuels, solid carbon, and ammonia for power generation [3-6].

DC-SOFC has received more and more attention in recent years. Andrew et al. [7] performed thermodynamic analyses of a gasification-driven direct carbon fuel cell (GD-DCFC). It was

found that the conversion efficiency of GD-DCFC was much higher than that of an auto-thermal gasification-based system. Their un-optimized system reached 220mW cm^{-1} at 0.68V operating voltage and 1178K operating temperature. Johnson et al. [8] developed a finite-element model for tubular carbon fuel cells to study the effects of design parameters (i.e. tube spacing and operating potential) on the power output of the fuel cell. It was found that a relatively high power density (170mW cm^{-2}) could be achieved with a cell efficiency of higher than 50%. Alexander et al. [9,10] proposed a steam-carbon-air fuel cell for H_2 and electricity co-generation. A high efficiency of above 78% was achieved for H_2 and electricity co-generation. They also found that CO oxidation kinetics contributed significantly to steam reduction. Bai et al. [11] assembled and tested a 3-cell-stack direct carbon solid oxide fuel cell (DC-SOFC) and achieved a peak power density of 465 mW cm^{-2} at 850℃. They also proposed to develop DC-SOFC into a high performance battery based on their experimental results. Gur et al. [12] proposed the reaction mechanisms of DC-SOFC were: Boudouard reaction between C and by CO_2 to produce CO and electrochemical oxidation of CO at the triple phase boundary (TPB) of SOFC. Xie et al. [13] experimentally verified the reaction mechanism of a DC-SOFC proposed by Prof. Gur by comparing the performance of a DC-SOFC with an SOFC operated on pure CO. Xie et al. [13] also did experiments for gas-electricity co-generation through a DC-SOFC. It was found that the overall efficiency for gas-electricity co-generation was almost twice of the electrical conversion efficiency and a rapid rate of the Boudouard reaction was very important to get high electricity power and CO production rate in a DC-SOFC. Yang et al. [14] fabricated a carbon-air battery based on an SOFC integrated with a ceramic CO_2-permeable membrane. A peak power density of 279.3

mW cm^{-2} was achieved at 850℃ and continuously operated a small stack composed of two batteries for 200 min. Chen et al. [15] proposed a novel power system integrating coal gasification with SOFC and chemical looping combustion. A high power efficiency of 49.8% was achieved with complete CO_2 separation. In another study by Nease and Adams [16], life cycle analyses of bulk-scale coal-fueled solid oxide fuel cell power plants were conducted. It was found that with carbon capture and storage (CCS) system, the coal-fueled SOFC power plant could make a much lower environmental impact than the most modern plants using natural gas. The study shows the potential of carbon-based SOFC for a sustainable future.

1.2. Unsolved problems and the need of the present study

The above-mentioned studies demonstrated the high efficiency and feasibility of gas-electricity cogeneration of DC-SOFC. However, most of them are experimental research and only some preliminary modeling studies are available. The current literature is lacking a detailed analysis on the physical/chemical processes in a DC-SOFC. In practice, the carbon fuel may be located at a certain distance away from the DC-SOFC anode. The effect of this distance on the DC-SOFC performance is still unknown but it is an important factor for practical and large-scale application of DC-SOFCs. The previous studies on DC-SOFC employed the electrolyte-supported configuration [1]. However, previous modeling studies on H_2-fueled SOFC suggested that anode-supported configuration is optimal for SOFC [17, 18]. It is unknown whether the anode-supported configuration for DC-SOFC is favorable or not, as the chemical and electrochemical reactions in the porous anode of a DC-SOFC are more complicated than a conventional SOFC running on gaseous fuels. In addition, the characteristics of CO generation from the DC-SOFC have not been well studied and understood

yet.

In order to fill the above-mentioned research gap, a 2D mathematical model is developed for an axisymmetric-tubular DC-SOFC. The model is validated with the experimental data on DC-SOFC. Detailed parametric simulations are conducted to understand the complex physical/chemical processes in the DC-SOFC with a focus on the CO and electricity cogeneration characteristics. Effects of the distance between solid carbon and anode on the DC-SOFC performance and different kinds of supported layer of the cell are studied. Electricity and CO cogeneration by DC-SOFC for practical applications is also discussed.

2. Model development

2.1. Model assumption and calculation domain

A 2D numerical model is developed to describe the electrochemical/chemical reactions, ion/electron transport, mass transport and momentum transport in a tubular DC-SOFC. In the literature, Liu et al.'s work [1] on DC-SOFC provided detailed experimental setup and operating conditions, such as the materials used, the operating temperature, the thickness of cell components, etc. In their study, the current-potential (I-V) characteristics of an electrolyte-supported tubular SOFC were measured. So their cell configuration is used for the present model and their measured results are used for model validation.

The schematic of the electrolyte supported tubular DC-SOFC is shown in Fig. 1(a). Activated carbon is supplied to the anode chamber and air is supplied to the cathode channel. The initial O_2 in the anode chamber reacts with the activated carbon to produce CO_2, which reacts with

carbon through the Boudouard reaction to form CO. The produced CO molecules diffuse into the porous anode and reacts with O^{2-} at the triple phase boundary (TPB) to form CO_2 molecules, which subsequently diffuse back from the TPB to the anode chamber to react with the carbon fuel for CO generation. These processes repeat between the anode chamber and the porous anode to produce CO and generate electricity as shown in Eqs. (1, 3-5).

The electrochemical part of the cell has a length of 9mm (L_{cell}), an inner diameter of 11.518mm and an outer diameter of 12mm. The thicknesses of the anode, electrolyte and cathode are 20μm, 201μm and 20μm, respectively. The thicknesses of anode and electrolyte are exchanged when the anode-supported configuration is considered. The modeled tubular DC-SOFC uses Ag-GDC composites (mixture of GDC (gadolinium doped ceria, $Ce_{0.8}Gd_{0.2}O_{1.9}$) and silver) as both electrodes and YSZ (yttrium stabilized zirconium) as electrolyte. The two electrodes are porous enough for gas transport and the electrolyte is dense enough to be gas-tight. The current density is measured at operating potentials ranging from 0.2 V to 0.9 V.

The main assumptions are shown below.

(1) The electrochemical reactions spatially take place along the electrode thickness within the porous electrode. The electrochemical reaction active sites are assumed to be uniformly distributed in the porous electrodes. The two conducting phases (electronic and ionic) in the porous electrodes are continuous and homogeneous.

(2) The ionic and electronic charge transport processes take place in the PEN (Positive Electrode-Electrolyte-Negative electrode assembly). The charge transfer reaction can take place at TPB throughout the porous electrode.

(3) All gases (CO, CO_2, H_2, H_2O, O_2 and N_2) are ideal gases. The gas flow is incompressible.

(4) Temperature distribution in the DC-SOFC is uniform due to the small size of the modeled cell.

(5) The volume of activated carbon fuel in the anode chamber does not change with time.

2.2. Governing equations

The 2D numerical model fully considers the electrochemical/chemical reactions, ion/electronic charge transport, mass and heat transfer processes. The 2D model consists of the following sub-models: chemical reaction model, electrochemical reaction model, mass transport model and fluid flow model.

2.2.1. Chemical reaction model

The chemical reaction model is used to calculate the reaction rate of the reversed Boudouard reaction in the anode chamber:

$$C + CO_2 = 2CO \tag{1}$$

It should be noted that the initial CO_2 comes from the oxidation of carbon by the initial O_2 in the anode. When the DC-SOFC is in operation, CO_2 is continuously produced from the electrochemical reaction. The rate of reversed Boudouard reaction (R_{rb}) can be obtained as [19]:

$$R_{rb} = k_{rb}\exp(-E_{rb}/RT)c_{CO_2} \tag{2}$$

2.2.2. Electrochemical reaction model

The electrochemical reaction model is developed to compute the electrochemical reaction rate (related to current density) at given operating potential. As shown in Fig.1, the gas mixture of CO/CO_2 flows in the anode while air is supplied to the cathode. In the porous cathode, O_2 molecules diffuse through the porous cathode to the TPB, where they are reduced to oxygen ions (O^{2-}) via reactions (3).

$$O_2 + 4e^- \rightarrow 2O^{2-} \tag{3}$$

The oxygen ions transport through the dense electrolyte to TPB in the anode, where they electrochemically react with CO molecules to generate electrons and CO_2:

$$2CO + 2O^{2-} \rightarrow 2CO_2 + 4e^- \tag{4}$$

The overall electrochemical reaction can be obtained by combining Eq. (3) and Eq. (4) as:

$$2CO + O_2 \rightarrow 2CO_2 \tag{5}$$

The operating potential from the DC-SOFC can be determined using the equilibrium potential and the various overpotential losses:

$$V = E + \eta_{act,an} + \eta_{act,ca} + \eta_{ohmic} \tag{6}$$

E is the equilibrium potential (Nernst potential) when the current density is 0. η_{act} is the activation overpotential reflecting the energy barrier needed for the electrochemical reaction to proceed. η_{ohmic} is the ohmic overpotential related to the ionic/electronic conduction. The concentration overpotentials are not explicitly included in Eq. 6 as they are included in the equilibrium potential calculation.

2.2.2.1. Equilibrium potential (Nernst potential)

In the DC-SOFC, the equilibrium potential for reactions (5) can be determined by Eq. (7) [20]. The concentration overpotentials are included in the equilibrium potential as the gas partial pressures at the reaction sites are used in the calculation.

$$E_{CO} = E_{CO}^{0} + \frac{RT}{2F}\ln\left[\frac{P_{CO}^{L}(P_{O_2}^{L})^{1/2}}{P_{CO_2}^{L}}\right] \quad (7)$$

E^0 is the potential under standard conditions. R is the universal gas constant (8.3145 $Jmol^{-1}K^{-1}$). T is the operating temperature (K). F is the Faraday constant (96485 $Cmol^{-1}$). P_{CO}^{L}, $P_{CO_2}^{L}$ and $P_{O_2}^{L}$ are the local partial pressures of CO, CO_2 and O_2 at the TPB (reaction sites), respectively. The value of E^0 for CO fuel at a temperature between 600K and 1200K can be calculated by Eq. (8)[21]:

$$E_{CO}^{0} = 1.46713 - 0.0004527T \quad (8)$$

Thus, the Nernst potential can be calculated by combining Eq. (7) and Eq. (8) as:

$$E_{co} = 1.46713 - 0.0004527T + \frac{RT}{2F}\ln\left[\frac{P_{CO}^{L}(P_{O_2}^{L})^{1/2}}{P_{CO_2}^{L}}\right] \quad (9)$$

2.2.2.2. Activation overpotential

Activation overpotential is the energy loss involved in the electrochemical reaction, which is related to the electrode kinetics at the reaction site. The Butler-Volmer (BV) equation is a general expression relating the activation overpotential with the current density for an electrochemical system. The BV equation is applicable to not only H_2 fuel cells, but also fuel

cells using alternative fuels. In our previous studies on SOFC considering CO as an electrochemical fuel, the general BV equation has been applied to determine the activation loss [6, 21].

$$i = i_0 \left\{ \exp\left(\frac{\alpha n F \eta_{act}}{RT}\right) - \exp\left(\frac{(1-\alpha) n F \eta_{act}}{RT}\right) \right\} \quad (10)$$

Here i_0 is the exchange current density representing the activity of the electrode. α is the electronic transfer coefficient and *n* is the number of electrons transferred per electrochemical reaction.

2.2.2.3. Ohmic overpotential

The ohmic overpotential in the DC-SOFC is caused by electron/ion conduction. The ionic conductivity of the electrolyte and the ionic/electronic conductivities of the electrodes are summarized in Table 1. The ohmic overpotential can be calculated with the Ohm's law:

$$i_l = -\sigma_l{}^{eff} \nabla(\emptyset_l) \quad (11)$$

$$i_s = -\sigma_{s.eff} \nabla(\emptyset_s) \quad (12)$$

Here $\sigma_{l.eff}$and $\sigma_{s.eff}$ are the effective ionic and electronic conductivities. $\emptyset_l$ and $\emptyset_s$ are the ion conducting and electron conducting electric potentials, respectively. In the porous electrodes, the effective conductivities are related to the structural parameters including volume fraction and tortuosity.

$$\sigma_l{}^{eff} = \sigma_l \cdot \frac{V_l}{\tau_l} \quad (13)$$

$$\sigma_s{}^{eff} = \sigma_s \cdot \frac{V_s}{\tau_s} \quad (14)$$

Here σ_l and σ_s are the intrinsic ionic and electronic conductivities, whose values are

summarized in Table 1.

2.2.3. Mass transport model

In the porous electrodes of DC-SOFC, both free molecular diffusion and Knudsen diffusion are considered. Free molecular diffusion dominates in large pores and Knudsen diffusion becomes significant when the pore sizes are comparable or smaller than the molecular mean-free path. The extended Fick's model is used to describe gas transport in the porous electrodes as:

$$N_i = -\frac{1}{RT}\left(\frac{B_0 y_i P}{\mu}\frac{\partial \mathrm{P}}{\partial \mathrm{z}} - D_i^{eff}\frac{\partial (y_i \mathrm{P})}{\partial \mathrm{z}}\right) \quad (i = 1, \dots, n) \tag{15}$$

where N_i represents the flux of mass transport, B_0 is the permeability coefficient, y_i is the molar fraction of component i, μ is the dynamic viscosity of the gas mixture and D_i^{eff} is the effective diffusivity of species *i*. The effective diffusion coefficient (D_i^{eff}) considering both molecular diffusion coefficient (D_{im}^{eff}) and Knudsen diffusion coefficient (D_{ik}^{eff}) can be calculate as:

$$D_i^{eff} = \left(\frac{1}{D_{im}^{eff}} + \frac{1}{D_{ik}^{eff}}\right) \tag{16}$$

D_{im}^{eff} and D_{ik}^{eff} depend on the micro-structure of the porous electrode and operating conditions. The detailed calculation procedures of these two parameters can be found in references [22, 23].

2.2.4. Fluid flow model

The general Navier-Stokes (N-S) equation is used to describe the momentum conservation. In the gas channels, the N-S equation can be described as:

$$\rho\frac{\partial u}{\partial t}+\rho u\nabla u=-\nabla p+\nabla[\mu\left(\nabla u+(\nabla u)^{T}\right)-\frac{2}{3}\mu\nabla u\Big] \quad (17)$$

In the porous electrodes and the anode chamber, the N-S equation is modified by including the Darcy's term for momentum conservation:

$$\rho\frac{\partial u}{\partial t}+\rho u\nabla u=-\nabla p+\nabla[\mu\left(\nabla u+(\nabla u)^{T}\right)-\frac{2}{3}\mu\nabla u\Big]-\frac{\varepsilon\mu u}{k} \quad (18)$$

where ρ is the local gas density (kg.m^{-3}) which is related to gas partial pressure, temperature and differs from inlet to outlet, μ is dynamic viscosity of fluid (kg.m^{-1}.s^{-1}), u is the velocity vector, p is pressure and ε is the porosity of the electrode. The values of ρ and μ can be determined from Eqs. (19)-(21) [24].

$$\rho=\frac{1}{\sum_{i=1}^{N}Y_i/\rho_i} \quad (19)$$

$$\mu=\sum_{i=1}^{n}\frac{y_i\mu_i}{\sum_{j=1}^{n}y_j\varphi_{ij}} \quad (20)$$

$$\varphi_{ij}=\sqrt{\frac{M_j}{M_i}}=\varphi_{ji}^{-1} \quad (21)$$

where ρ_i is the density of gas species *i* and M_i is molecular weight of species *i* (kg.kmol^{-1}).

2.3. Boundary conditions

2.3.1. Electrochemical reaction

The electric potentials are specified at the outer boundaries of cathode and anode as working potential and zero potential, respectively. The insulation condition is applied to the bottom

and top of the cell.

2.3.2. Mass transport

Inflow gas molar fraction is specified at the inlet of the cathode. The convective flux boundary condition is specified at the outlets of the cathode and anode. Zero flux is assumed at the end of anode chamber, electrolyte/electrode interface and the ends of electrodes.

2.3.4. Fluid flow

Standard gas flow rate (standard cubic centime per minute: SCCM) is specified at the cathode and pressure condition is specified at the outlet. No-slip condition is applied to the end of anode chamber, electrolyte/electrode interface and the ends of electrodes.

2.4. Model parameters

For model validation, the values of material properties and operation parameters are set to be the same as the experimental conditions in ref. [1] as shown in Table 1, Table 2 and Table 3. The electrochemical characteristics of the model are validated with the experimental data using H_2 as a fuel for SOFC. The exchange current density for CO oxidation in DC-SOFC ($i_{0,co}$) is assumed to be 0.45 times that of H_2 oxidation in a H_2-fueled SOFC. The rate of Boudouard reaction depends on reaction area and activity of catalyst. These effects are fully considered by tuning the equilibrium parameter (k_{rb}). In the parametric simulations, the parameters are varied to evaluate their effects on the DC-SOFC performance. The tuning parameters used for the base-case simulation are summarized in Table 4.

2.5. Model solution

The model is solved at certain cell potential, inlet gas flow rate, inlet gas species molar fraction, and temperature. The outputs of the model are the distributions of current density, species concentration, chemical reaction rates and others. The calculations are performed using the finite element commercial software COMSOL MULTIPHSICS®.

3. Results and discussion

3.1. Model evaluation

In this section, the modeling results of current-potential characteristics are compared with experimental data for model validation. The model tuning parameters are summarized in Table 4. The comparison between simulation and experiment is shown in Fig. 2. The quite small difference between the modeling results and experimental data validates the present model. In the subsequent parametric simulations, the same DC-SOFC structural parameters and tuning parameters are used but the operation temperature, potential and the distance between the carbon chamber and the porous anode (D_{ce}) are changed to investigate their effects on the DC-SOFC performance.

3.2. Effect of distance between carbon and anode

In the DC-SOFC, CO for electrochemical reaction comes from Boudouard reaction between carbon and CO_2. Since CO_2 is produced from the electrochemical reaction in steady-state operation, the counter-diffusion of CO and CO_2 between the carbon chamber and the TPB in

the porous anode could be a limiting factor for DC-SOFC performance under certain conditions. As the distance between carbon chamber and anode electrode could play an important role, both the absolute value of D_{ce} and relative value of D_{ce} ($R_{ce} = D_{ce}/L_{cell}$) are studied and discussed in this section. The effects of D_{ce} on DC-SOFC performance are shown from Fig. 3 to Fig. 5. The detailed operation conditions are shown in Table 5.

The output current density of DC-SOFC is found to increase with decreasing D_{ce} (Fig. 3a). The distance effect is more pronounced at a low operating potential (or high current density) but is small at a high operating potential. This phenomenon is caused by both gas transport and electrochemical reaction kinetics. As can be seen from Fig. 4, the molar fraction of CO in the carbon chamber is very high (>0.89) with D_{ce} values. When D_{ce} is very small ($D_{ce} = 59\mu m,\ R_{ce} = 0.007$), the CO fraction in the porous anode is also high and very close to that in the carbon chamber. With increasing D_{ce} ($D_{ce} = 4559\mu m,\ R_{ce} = 0.51$), the transport of CO from the carbon chamber to the TPB in the porous anode becomes difficult. Thus, the molar fraction of CO in the porous anode decreases with increasing D_{ce}. When the DC-SOFC is operated at a lower potential (0.2V), the current density is higher and more CO is consumed by electrochemical reaction at the TPB in the porous anode, which causes significant concentration gradient of CO in the porous anode. Consequently, the performance reduction of DC-SOFC is larger at a lower operating potential and at a larger D_{ce}.

It should be noted that although the performance of DC-SOFC decreases with increasing D_{ce}, the performance is still very good even at a large D_{ce} ($D_{ce} = 4559\mu m,\ R_{ce} = 0.51$), as can be seen from Fig. 3b. This result indicates that it is feasible to develop large-scale DC-SOFC system since the distance between carbon fuel and anode electrode does not reduce the DC-

SOFC performance too much.

It is also found that the current density increases slightly along the cell length in the DC-SOFC (Fig. 5). For comparison, the current density decreases significantly along the cell length when gaseous fuel like H_2 and CO is used in SOFC. This is because the CO fuel can be produced from the carbon chamber along the cell length in the DC-SOFC, which results in negligible CO concentration gradient along the channel. However, for H_2 or CO fueled SOFC, the electrochemical consumption of the fuel causes a large fuel concentration gradient along the channel, which results in decreased local equilibrium potential and current density along the cell length direction.

3.3. Effect of operating temperature

The effects of operating temperature on DC-SOFC are shown in Fig.6. The detailed operating conditions are shown in Table 6.

As expected, the current density of the DC-SOFC increases with increasing operating temperature (Fig. 6a). This is mainly due to the faster Boudouard reaction kinetics at a higher temperature, producing more CO from CO_2 and carbon for electrochemical reaction. In addition, the electrochemical reaction kinetics and the ionic conduction are both improved at a higher temperature. It can also be found from Fig. 6b that the molar fraction of CO at the anode outlet is quite high even at a large D_{ce}, when the DC-SOFC is operated at a high temperature (1273K). This result indicates that the CO molar fraction at the DC-SOFC outlet is high and controllable, which demonstrates the feasibility of using carbon fuel in DC-SOFC

for electricity and CO co-generation at a high temperature.

The performance of DC-SOFC with a large D_{ce} can also be improved by increasing temperature as can be seen in Fig. 6a. The performance of DC-SOFC with 4559 μm D_{ce} at 1223K is very close to that with a D_{ce} of 59μm at an operating temperature of 1123 K. This good performance of DC-SOFC is also benefited from the fast Boudouard reaction kinetics at a higher temperature. In addition, the CO molar fraction is much increased at a higher temperature in the DC-SOFC with large D_{ce}, which again indicates that the electricity and CO co-generation at an industry level by DC-SOFC could be feasible.

3.4. Comparison between electrolyte-supported and anode-supported DC-SOFC

In Liu et al.' work [1] and in the above simulations, the electrolyte-supported configuration is employed for the DC-SOFC. However, previous studies on SOFC suggested that the anode-supported configuration could offer better cell performance due to the greatly reduced ohmic loss and the only slightly increased concentration loss [25]. As the gas diffusion in the DC-SOFC is more complicated and is coupled with the Boudouard reaction, whether the anode-supported configuration is still the optimal configuration for DC-SOFC and how much performance improved can be achieved are still unknown. In this section, the performance of DC-SOFC with the anode-supported configuration is studied and compared with the electrolyte-supported case.

The schematic of anode supported DC-SOFC can be seen in Fig. 1 (b) and the detailed operating conditions are shown in Table 7.

The performance comparison between the electrolyte-supported DC-SOFC and the anode-supported DC-SOFC is shown in Fig. 7. The performance of the anode-supported DC-SOFC is much better than that of the electrolyte-supported DC-SOFC. This result means that the decrease in ohmic loss of the electrolyte is greater than the increase in concentration overpotential in the anode-supported DC-SOFC. In addition, it can be seen from Fig. 8a that the CO concentration from the anode-supported DC-SOFC is still very high even at a large current density (27500A m^{-2}) when D_{ce} is small (59μm). However, the CO concentration in anode is substantially decreased to be below 0.8 (Fig. 8b) when D_{ce} is large (4559μm) and the operating potential is small (0.2V). The results mean that the anode-supported configuration is beneficial for the electrical power output of the DC-SOFC but not favorable for CO generation. In order to improve the CO generation, a small D_{ce} and a relative high operating potential are recommended in anode-supported DC-SOFC.

4 Conclusions

A multi-physics model considering electrochemical reaction, chemical reactions, ionic/electronic charge transport, mass transport and momentum transport is developed to characterize the performance of a tubular DC-SOFC. The model is validated by comparing the simulation results with experimental data by Liu's group. Parametric simulations are conducted to evaluate the effects of distance between the carbon chamber and the porous anode on DC-SOFC performance. In addition, the temperature effect on DC-SOFC performance and the CO generation characteristics of the DC-SOFC are also studied.

It is found that the distance between carbon chamber and anode electrode D_{ce} could affect the performance of DC-SOFC to some extent. As D_{ce} is increased, the performance of DC-SOFC decreases. However, it is also observed that the performance of DC-SOFC with large D_{ce} is still good enough, indicating that the practical and large-scale DC-SOFC applications could be feasible.

The operating temperature significantly affects the DC-SOFC performance. At a high temperature, the molar fraction of CO at the outlet of DC-SOFC is high and it is feasible to convert the carbon fuel for electricity and CO co-generation. However, at a lower operating temperature, both the average current density and the CO molar fraction at the DC-SOFC outlet are decreased, primarily due to the low Boudouard reaction rate. This study clearly demonstrates the feasibility of controlling the CO generation from DC-SOFC for CO and electricity co-generation.

Compared with gaseous fuel-fed SOFC, the current density of DC-SOFC is found to slightly increase along the cell length, due to the generation of electrochemical fuel along the cell length by the Boudouard reaction.

Electrolyte-supported and anode-supported DC-SOFCs are also compared to understand the effects of support-type on the electrical power output and CO generation characteristics. It is found that an anode-supported DC-SOFC has a much better electrical power output than that of an electrolyte-supported DC-SOFC. However, the anode-supported configuration is not favorable for CO generation, especially at a large D_{ce}. To improve CO generation, small D_{ce} and relatively higher operation potential are recommended for an anode-supported DC-SOFC.

The results in this paper show the attractive possibility for gas and electricity cogeneration with DC-SOFCs. This kind of SOFC uses cheap fuel (solid carbon) to generate both CO and electricity, which has great economic advantages. The modeling results also indicate that a higher temperature, smaller D_{ce} and anode support SOFC is more favorable in real applications. The good performance of DC-SOFC at large D_{ce} further suggests its application in industry.

Acknowledgement

This research is supported by a grant of SFC/RGC Joint Research Scheme (X-PolyU/501/14) from Research Grant Council, University Grants Committee, Hong Kong SAR.

Nomenclature

Abbreviation

Ag-GDC	The mixture of silver and GDC
DC-SOFC	Solid oxide fuel cell direct using carbon as fuel
GDC	Gadolinium doped ceria, $Ce_{0.8}Gd_{0.2}O_{1.9}$
GD-SOFC	Gasification-driven direct carbon fuel cell
H_2-SOFC	Solid oxide fuel cell using H_2 as fuel
PEN	Positive Electrode-Electrolyte-Negative electrode assembly
SCCM	Standard cubic centime per minute
SOFC	Solid oxide fuel cell
TPB	Triple phase boundary
YSZ	Yttrium stabilized zirconium

Roman

D_{ce}	Distance between carbon and anode electrode
D_i^{eff}	Effective diffusivity of species i, $m^2 \cdot s^{-1}$
D_{ik}^{eff}	Knudsen diffusion coefficient of i, $m^2 \cdot s^{-1}$
D_{im}^{eff}	Molecular diffusion coefficient of i, $m^2 \cdot s^{-1}$
E	Equilibrium Nernst potential, V
E_a	Active energy, $J \cdot mol^{-1}$
F	Faraday constant, 96485 $C \cdot mol^{-1}$
i_o	Exchange current density, $A \cdot m^{-2}$
k	Reaction rate constant, in terms of m, mol, Pa and s
K_{br}	Equilibrium constant of Boudouard reaction
L_{cell}	Length of the cell, mm
n	Number of electrons transferred per electrochemical reaction
N_i	Flux of mass transport, $kg \cdot m^{-3} \cdot s^{-1}$
p	(partial) Pressure, Pa
R	Gas constant, 8.314 $J \cdot mol^{-1} \cdot K^{-1}$
R_{ce}	Ratio D_{ce} and cell length
T	Temperature, K
u	Velocity field, $m^3 \cdot s^{-1}$
v	Volume fraction

Greek letters

α	Charge transfer coefficient
β_{H_2}	Electrochemical kinetics parameter for H_2
ε	Porosity
η_{act}	Anode activation polarization, V
η_{ohmic}	Ohmic polarization, V
κ	Permeability, m^2
μ	Dynamic viscosity of fluid, Pa·s
ρ	Fluid density, $kg \cdot m^{-3}$
τ	Tortuosity
∅	Potential, V

Subscripts

an	Anode
ca	Cathode
co	Carbon monoxide
l	Ionic phase
s	Electronic phase

Superscripts

0	Parameter at equilibrium conditions
eff	Effective
L	Local

References

[1] Xie Y, Cai W, Xiao J, Tang Y, Liu J, Liu M. Electrochemical gas-electricity cogeneration through direct carbon solid oxide fuel cells. J Power Sources. 2015;277:1-8.

[2] Zheng KQ, Ni M. Reconstruction of solid oxide fuel cell electrode microstructure and analysis of its effective conductivity. Science Bulletin. 2016; 61(1): 78-85.

[3] Qu J, Wang W, Chen Y, Wang F, Ran R, Shao ZP. Ethylene glycol as a new sustainable fuel for solid oxide fuel cells with conventionl nickel-based anodes. Applied Energy. 2015; 148: 1-9.

[4] Duan NQ, Tan Y, Yan D, Jia L, Chi B, Pu J, Li J, Biomass carbon fueled tubular solid oxide fuel cells with molten antimony anode. Applied Energy. 2016; 165: 983-989.

[5] Jiao Y, Tian W, Chen H, Shi H, Yang B, Li C, Shao ZP, Zhu Z, Li SD. In situ catalyzed Boudouard reaction of coal char solid oxide-based carbon fuel cells with improved performance. Applied Energy. 2015; 141: 200-208.

[6] Ni M. Modeling and parametric simulations of solid oxide fuel cells with methane carbon dioxide reforming. Energ Convers Manage. 2013;70:116-129.

[7] Lee AC, Mitchell RE, Gür TM. Thermodynamic analysis of gasification-driven direct carbon fuel cells. J Power Sources. 2009;194:774-85.

[8] Johnson DU, Mitchell RE, Gür TM. Modeling Power Production in a Tubular Carbon Fuel Cell. ECS Transactions. 2014;61:235-43.

[9] Alexander BR, Mitchell RE, Gür TM. Steam-Carbon Fuel Cell Concept for Cogeneration of Hydrogen and Electrical Power. J Electrochem Soc. 2011;158:B505-B13.

[10] Alexander BR, Mitchell RE, Gür TM. Viability of Coupled Steam-Carbon-Air Fuel Cell Concept for Spontaneous Co-Production of Hydrogen and Electrical Power. J Electrochem Soc. 2012;159:F810-F8.

[11] Bai Y, Liu Y, Tang Y, Xie Y, Liu J. Direct carbon solid oxide Fuel Cell—a potential high performance battery. Int J Hydrogen Energ. 2011;36:9189-94.

[12] Li S, Lee AC, Mitchell RE, Gür TM. Direct carbon conversion in a helium fluidized bed fuel cell. Solid State Ionics. 2008;179:1549-52.

[13] Xie Y, Tang Y, Liu J. A verification of the reaction mechanism of direct carbon solid oxide fuel cells. Journal of Solid State Electrochemistry. 2012;17:121-7.

[14] Yang B, Ran R, Zhong Y, Su C, Tadé MO, Shao Z. A carbon-air battery for high power generation. Angewandte Chemie - International Edition. 2015;54:3722-5.

[15] Chen S, Lior N, Xiang W, Coal gasification integration with solid oxide fuel cell and chemical looping combustion for high-efficiency power generation with inherent CO2 capture. Applied Energy. 2015; 146: 298-312.

[16] Nease J, Adams II TA, Comparative life cycle analyses of bulk-scale coal-fueled solid oxide fuel cell power plants. Applied Energy. 2015; 150:161-175.

[17] Ni M, Leung MKH, Leung DYC, Parametric study of solid oxide fuel cell performance. Energy Conversion and Management. 2007. 48(5): 1525-1535.

[18] Chan SH, Xia ZT, Polarization effects in electrolyte/electrode-supported solid oxide fuel cells. Journal of Applied Electrochemistry. 2002. 32(3): 339-347.

[19] Mon E, Amundson NR. Diffusion and Reaction in a Stagnant Boundary Layer about a Carbon Particle. 2. An Extension. Industrial & Engineering Chemistry Fundamentals. 1978;17:313-21.

[20] Ni M. An electrochemical model for syngas production by co-electrolysis of H2O and CO2. Journal of Power Sources. 2012. 202:209-216.

[21] Ni M. Modeling of SOFC running on partially pre-reformed gas mixture. Int J Hydrogen Energ. 2012;37:1731-

1745.
[22] Zhang H, Chen J, Zhang J. Performance analysis and parametric study of a solid oxide fuel cell fueled by carbon monoxide. Int J Hydrogen Energ. 2013;38:16354-64.
[23] Ni M, Leung DYC, Leung MKH. Electrochemical modeling and parametric study of methane fed solid oxide fuel cells. Energ Convers Manage. 2009;50:268-278.
[24] Kakaç S, Pramuanjaroenkij A, Zhou XY. A review of numerical modeling of solid oxide fuel cells. Int J Hydrogen Energ. 2007;32:761-86.
[25] Suwanwarangkul R, Croiset E, Fowler MW, Douglas PL, Entchev E, Douglas MA. Performance comparison of Fick's, dusty-gas and Stefan–Maxwell models to predict the concentration overpotential of a SOFC anode. J Power Sources. 2003;122:9-18.
[26] Eguchi K, Setoguchi T, Inoue T, Arai H. Electrical-Properties of Ceria-Based Oxides and Their Application to Solid Oxide Fuel-Cells. Solid State Ionics. 1992;52:165-72.
[27] Luo Y, Shi Y, Li W, Cai N. Comprehensive modeling of tubular solid oxide electrolysis cell for co-electrolysis of steam and carbon dioxide. Energy. 2014;70:420-34.

List of Tables

Table.1 Model parameters

Parameters	**Value or expression**	**Unit**
Ionic conductivity		
GDC	$\frac{100}{T} \times 10^{(6.66071\ -\ \frac{5322.92}{T})}$ [26]	Sm^{-1}
YSZ	$3.34 \times 10^4 e^{\frac{-10300}{T}}$ [27]	Sm^{-1}
Electronic conductivity		
Ag	$\frac{1.59e^8}{(0.0038T-0.1134)}$	Sm^{-1}
Porosity		
Cathode	0.46	
Anode	0.46	
Electrode volume fraction		
GDC	0.21	
Ag	0.79	
S_{TPB}		
Cathode layer	2.14×10^5 [27]	m^2m^{-3}
Anode layer	2.14×10^5 [27]	m^2m^{-3}

Table. 2 Operation parameters for model validation (H_2-SOFC)[1]

Parameter	**Value**	**Unit**
Anode inlet gas flow rate for	50	SCCM
Cathode inlet gas flow rate	10	SCCM
Anode inlet gas composition	H_2(97%) + H_2O(3%)	
Cathode inlet gas composition	Air	
Temperature	1123	K

Table. 3 Operation parameters for model validation (DC-SOFC)[1]

Parameter	**Value**	**Unit**
Anode inlet gas flow rate	**0**	
Distance between anode chamber and electrode, D_{ce}	**59**	**μm**
Cathode inlet gas flow rate	10	SCCM
Cathode gas composition	Air	
Temperature	1123	K

Table. 4 Model tuning parameters

Parameter	**Value**	**Unit**
Cathode tortuosity	3	
Anode tortuosity	3	
H_2 exchange current density, i_{H_2}	1000	Am^{-2}
O_2 exchange current density i_{O_2}	400	Am^{-2}
CO exchange current density, i_{CO}	450	Am^{-2}
H_2 charge transfer coefficient, α_{H_2}	0.5	
CO charge transfer coefficient, α_{CO}	0.5	
O_2 charge transfer coefficient, α_{O_2}	0.5	
Equilibrium constant of Boudouard reaction	6×10^{13}	1/s

Table. 5 Operation parameters for D_{ce} effect study in DC-SOFC

Parameter	**Value**	**Unit**
Operating potential	0.2 - 0.9	V
Anode inlet gas flow rate	0	
Distance between anode chamber and electrode, D_{ce}	59 - 4559	μm
Cathode inlet gas flow rate	10	SCCM
Cathode gas composition	Air	
Temperature	1123	K

Table. 6 Operation parameters for temperature effect study in DC-SOFC

Parameter	**Value**	**Unit**
Operating potential	0.7	V
Anode inlet gas flow rate	0	
Distance between anode chamber and electrode, D_{ce}	59 - 4559	µm
Cathode inlet gas flow rate	10	SCCM
Cathode gas composition	Air	
Temperature	973 - 1273	K

Table. 7 Operation parameters for anode supported DC-SOFC

Parameter	**Value**	**Unit**
Operating potential	0.2 – 0.9	V
Anode inlet gas flow rate	0	
Distance between anode chamber and electrode, D_{ce}	59, 4559	µm
Cathode inlet gas flow rate	10	SCCM
Cathode gas composition	Air	
Temperature	1123	K

List of Figures

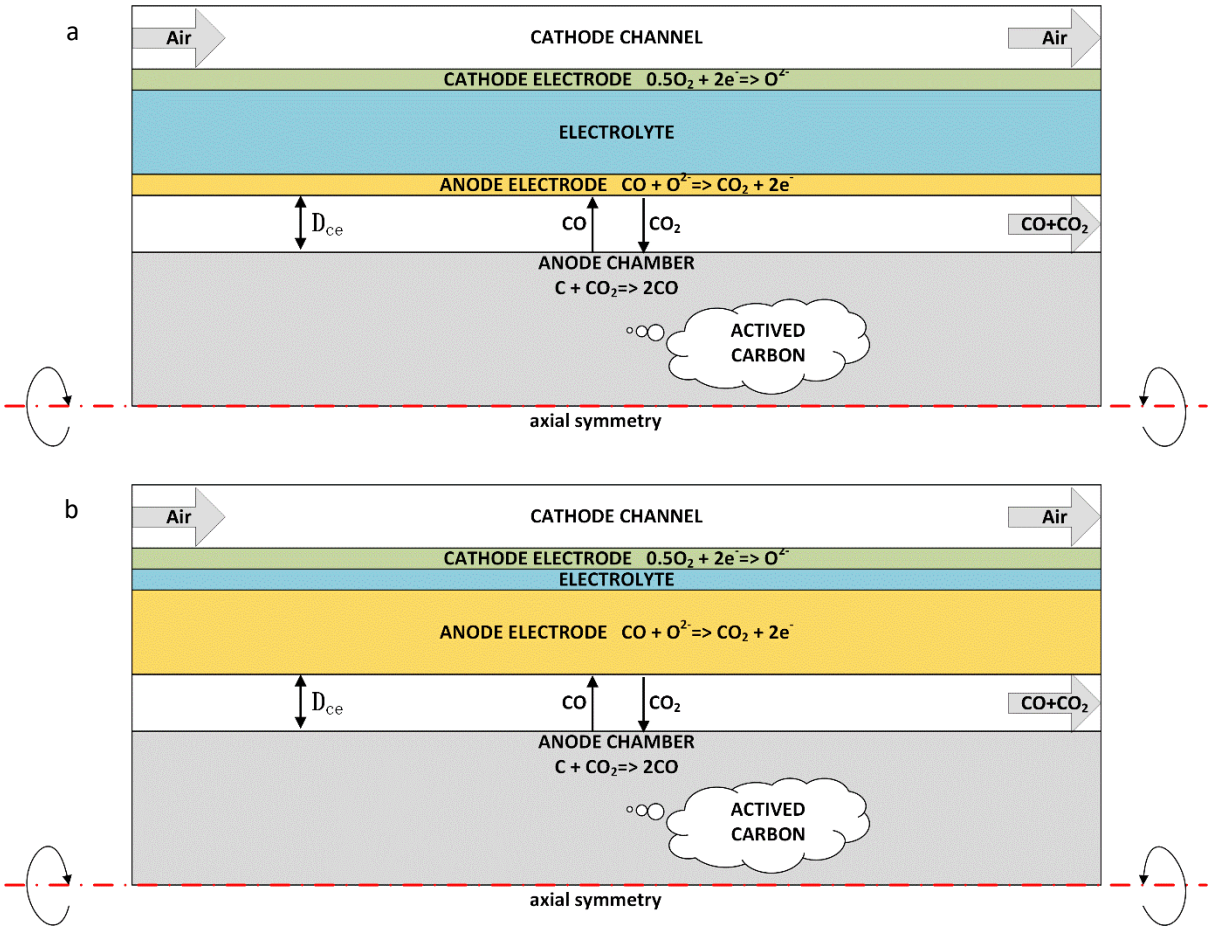

Fig.1. Schematic of (a) electrolyte supported DC-SOFC, (b) anode supported DC-SOFC

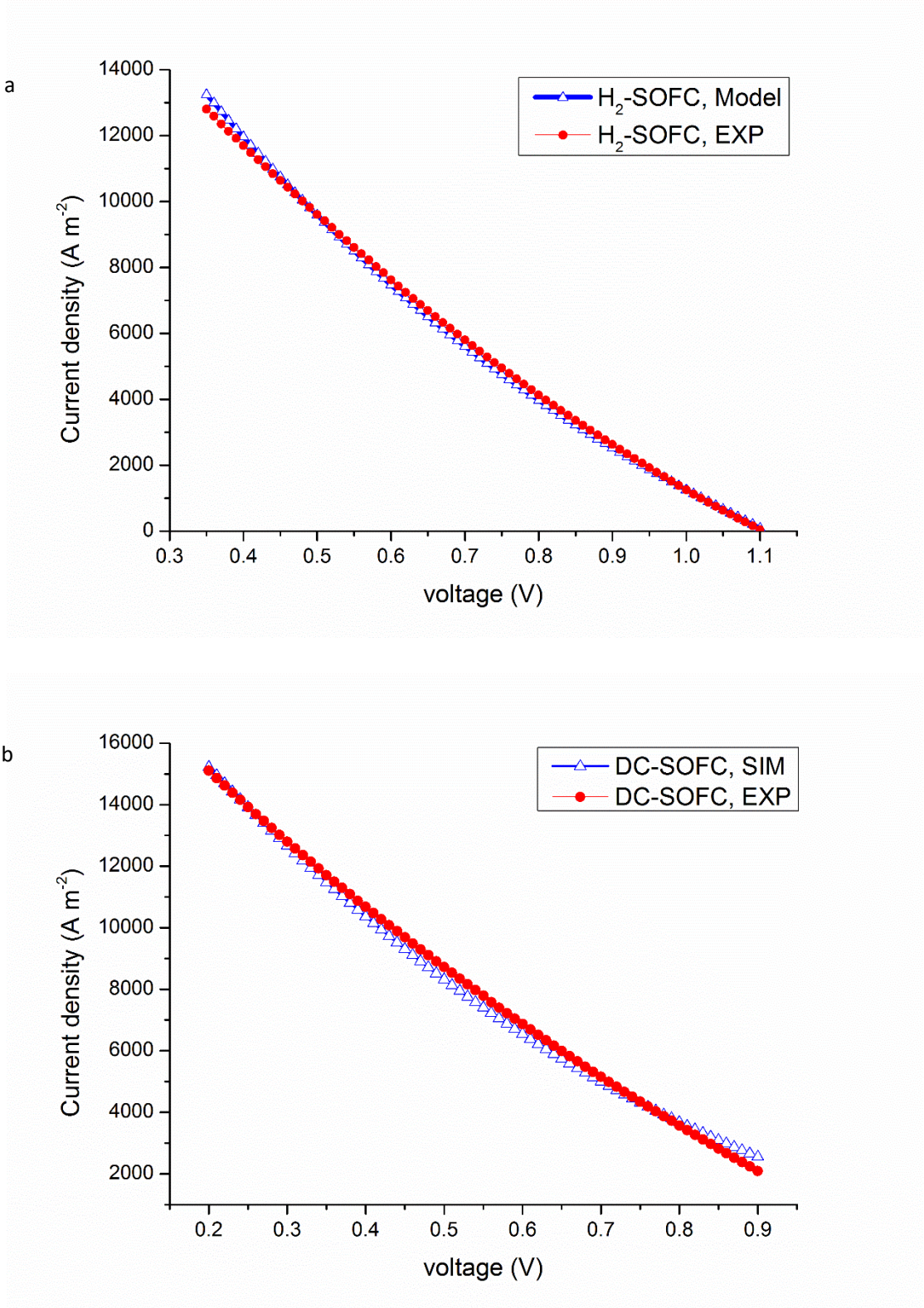

Fig.2 Model validation for (a) H_2-SOFC and (b) DC-SOFC

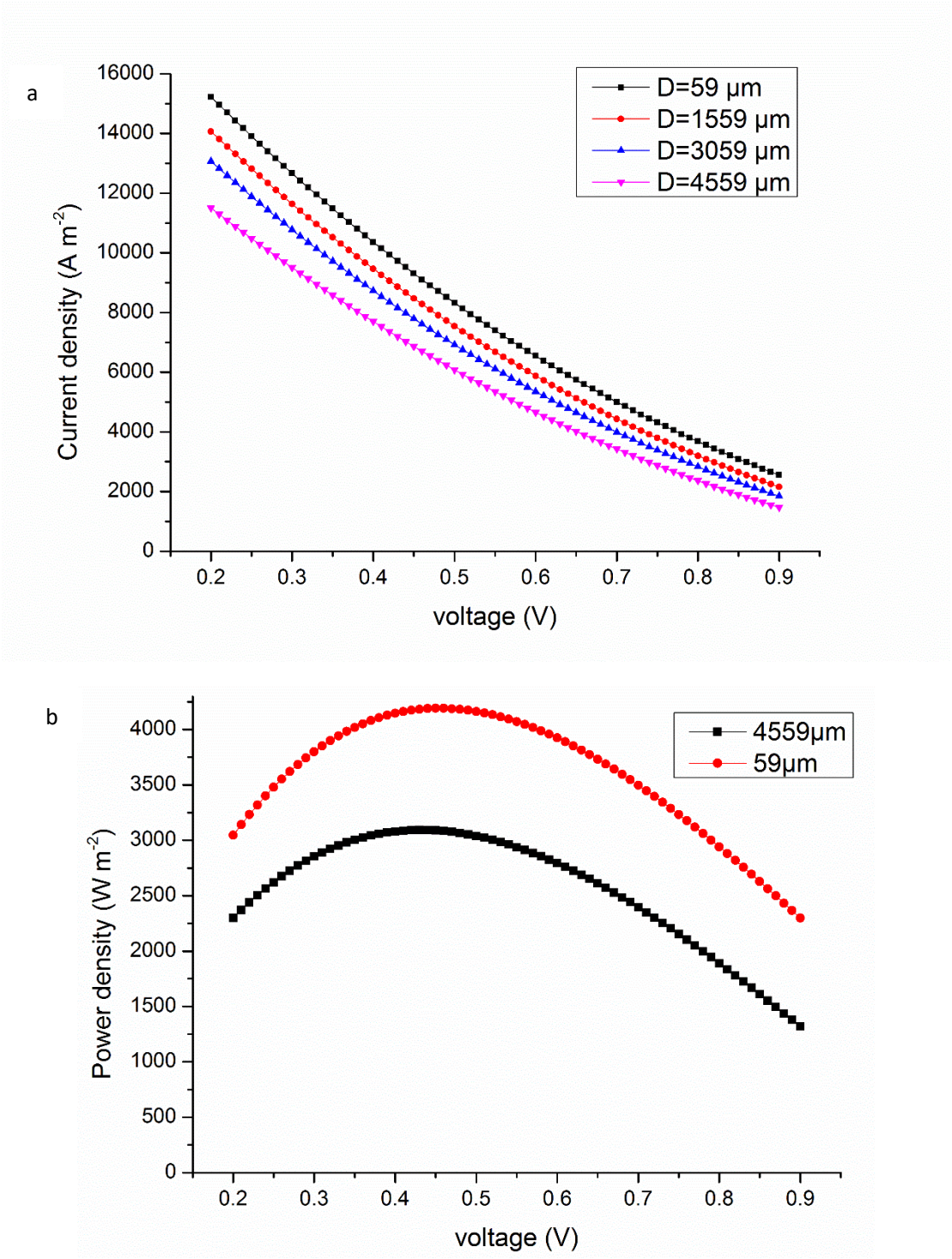

Fig.3. Effect of D_{ce} on (a) DC-SOFC output current density, (b) output power density at 1123K.

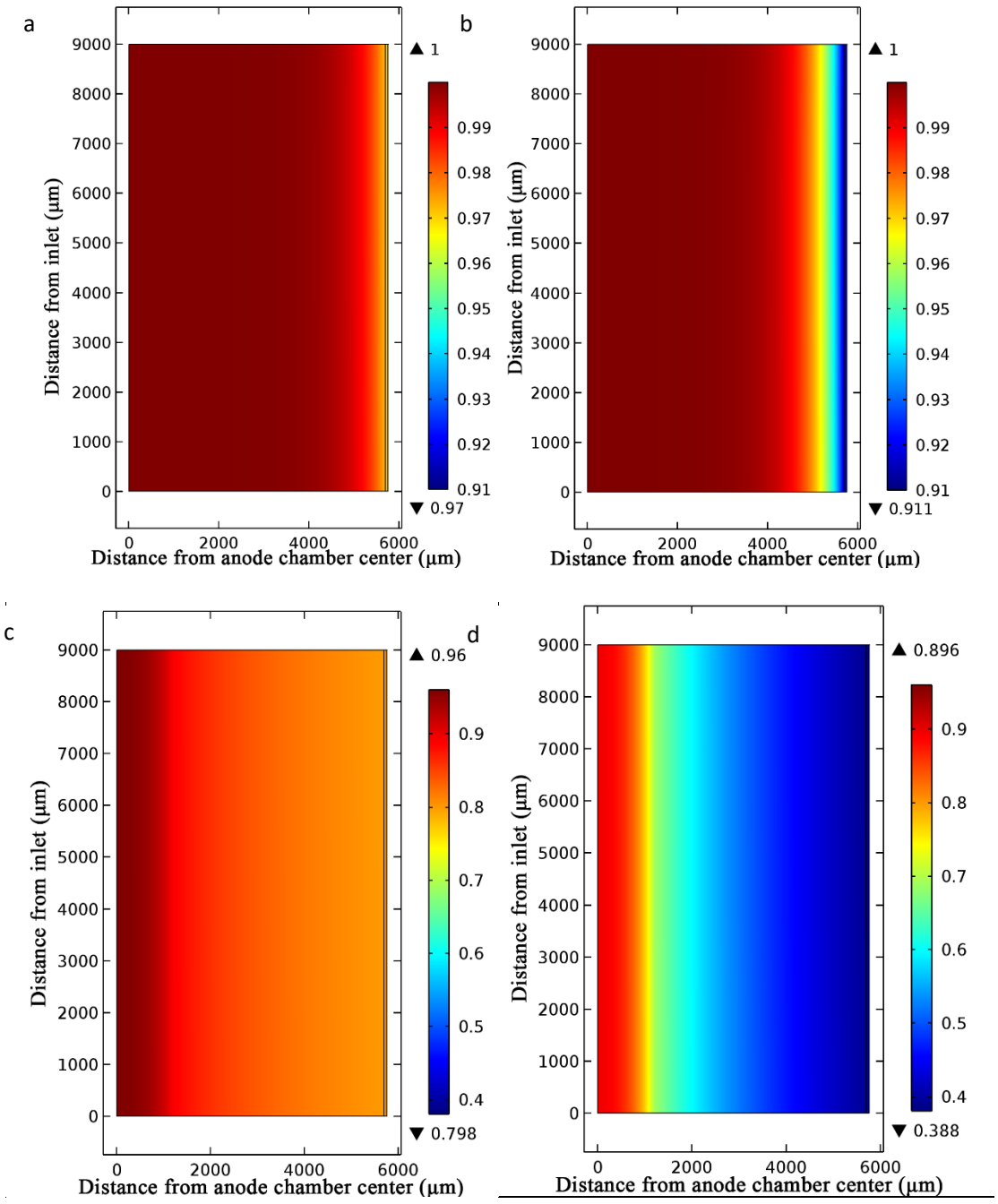

Fig.4. Effect of operating potential and D_{ce} on CO molar fraction distribution in DC-SOFC anode at 1123K: (a) $D_{ce} = 59\ \mu m, V = 0.7V$ (b) $D_{ce} = 59\ \mu m, V = 0.2V$ (c) $D_{ce} = 4559\ \mu m, V = 0.7V$ (d) $D_{ce} = 4559\ \mu m, V = 0.2V$

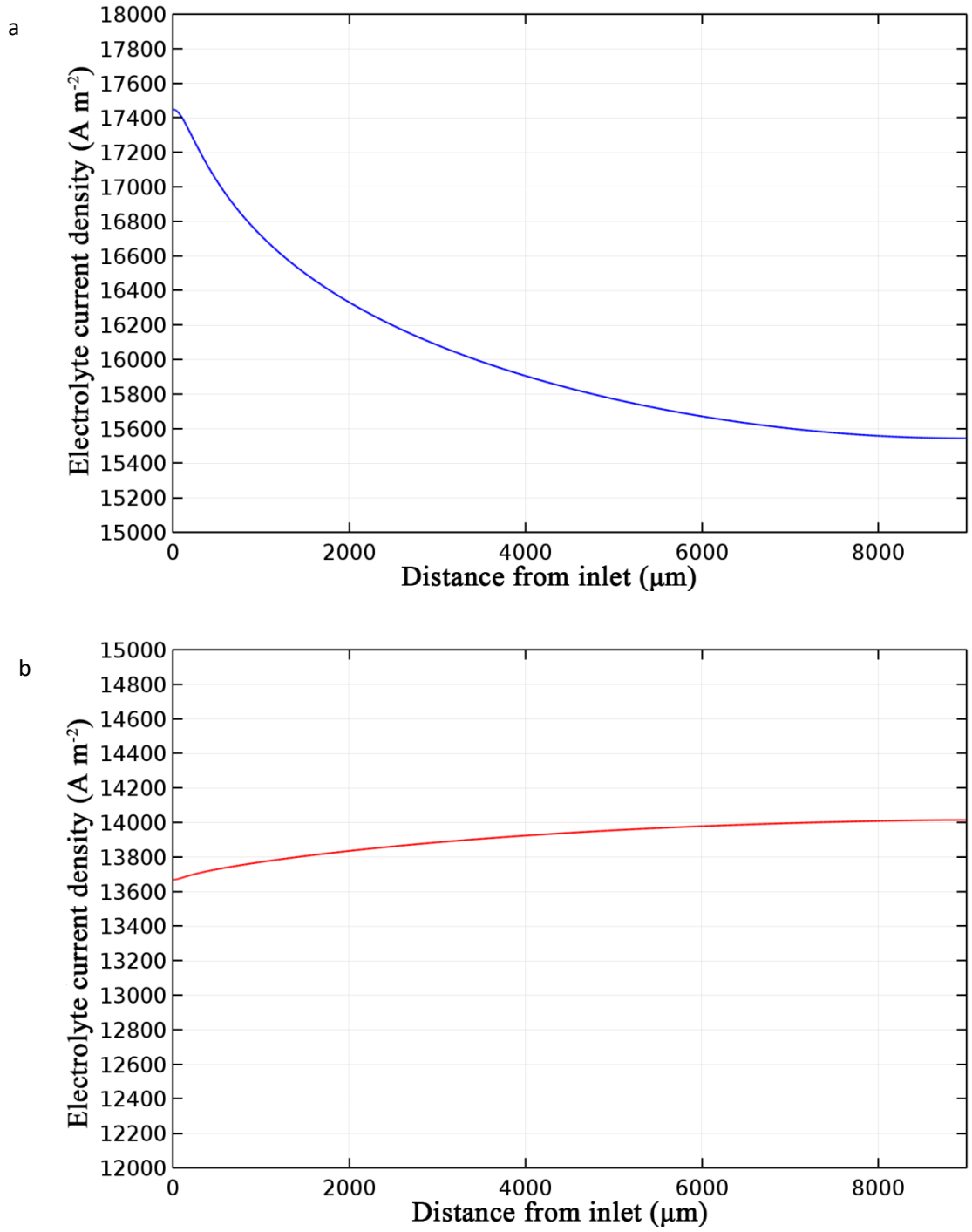

Fig.5. Current density distribution along electrolyte in (a) H_2-SOFC and (b) DC-SOFC

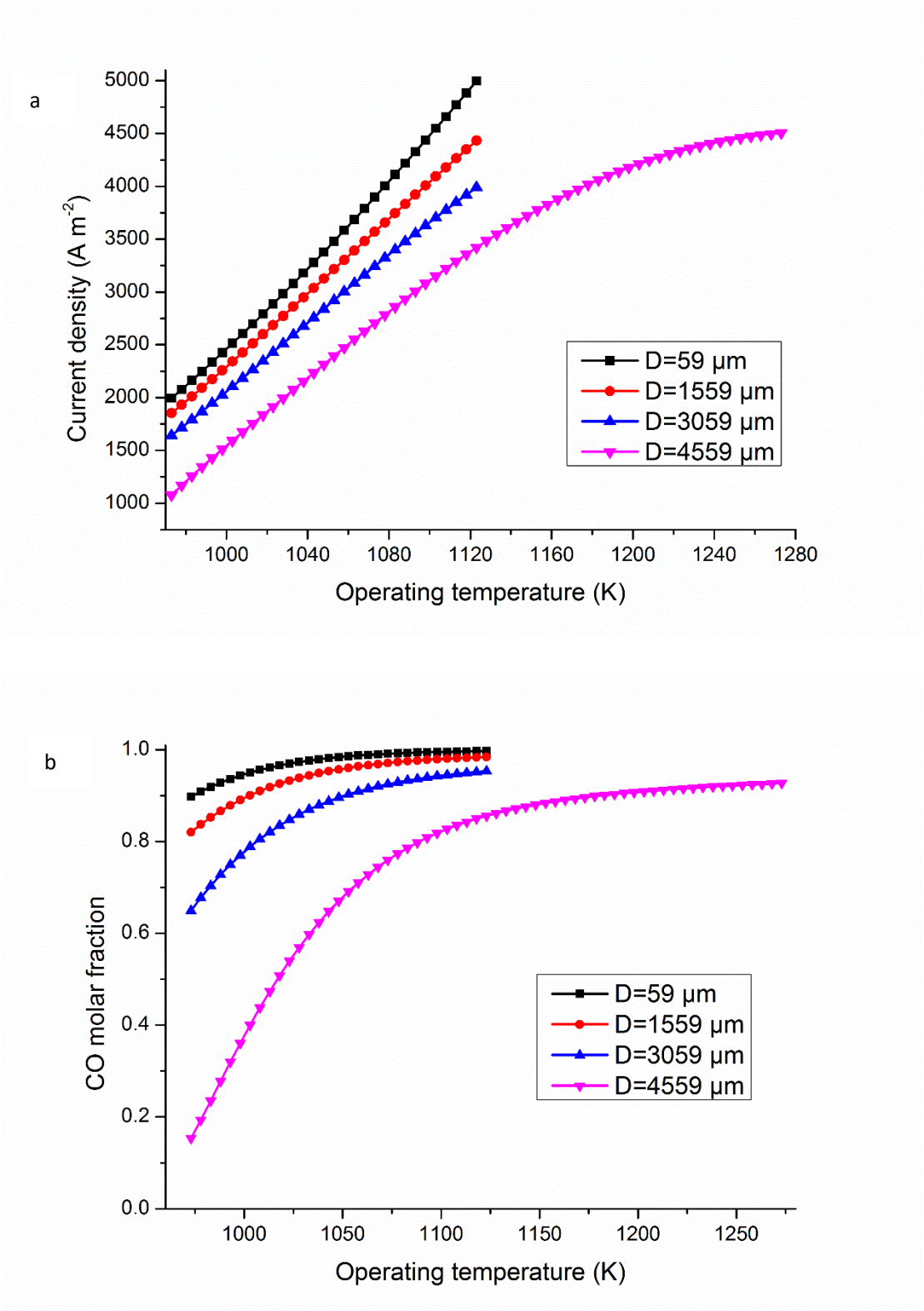

Fig.6. Effect of temperature on (a) output current density, (b) anode outlet CO molar fraction at 0.7 V operating potential and different D_{ce} cases.

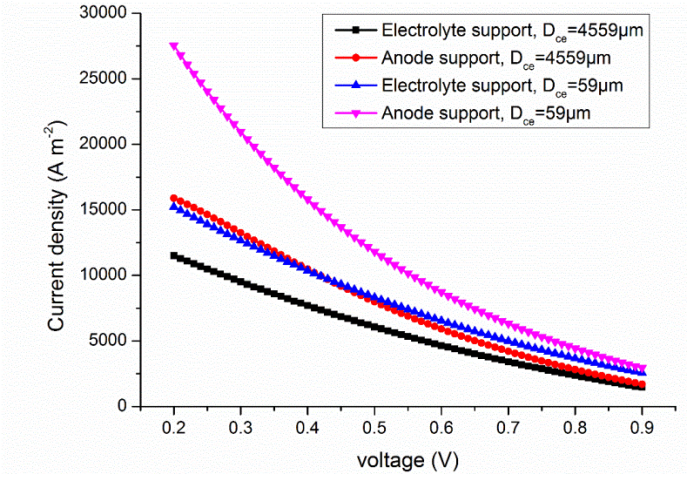

Fig.7 Performance comparison between electrolyte-supported and anode-supported DC-SOFCs at different D_{ce}

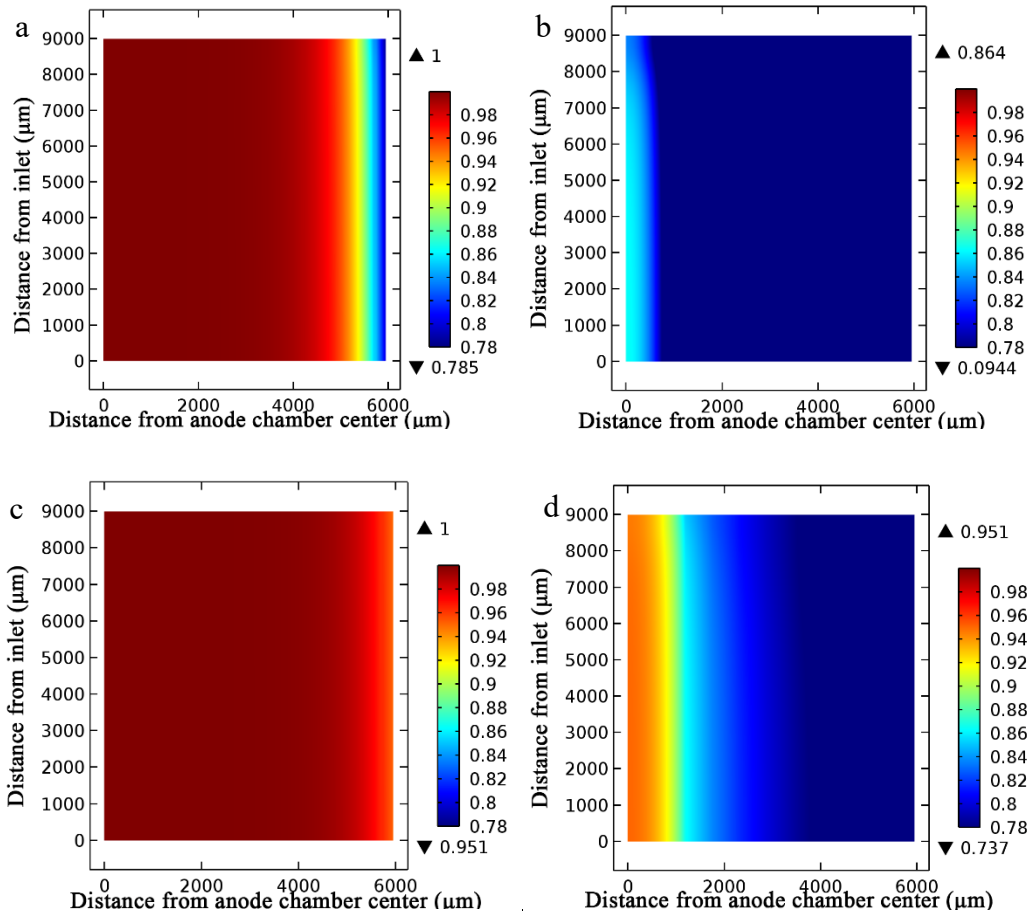

Fig.8. Effect of operating potential and D_{ce} on CO molar fraction distribution in anode supported DC-SOFC at 1123K: (a) $D_{ce} = 59$ μm, V = 0.2V (b) $D_{ce} = 4559$ μm, V = 0.2V (c) $D_{ce} = 59$ μm, V = 0.7V (c) $D_{ce} = 4559$ μm, V = 0.7V